MODELLING BINARY ALLOY SOLIDIFICATION BY A RANDOM PROJECTION METHOD

Sabrina Carpy, Hélène Mathis

MODELLING BINARY ALLOY SOLIDIFICATION BY A RANDOM PROJECTION METHOD

SABRINA CARPY AND HÉLÈNE MATHIS

ABSTRACT. This paper adresses the numerical modelling of the solidification of a binary alloy which obeys a liquidus-solidus phase diagram. In order to capture the moving melting front, we introduce a Lagrange projection scheme based a random sampling projection. Using a finite volume formulation, we define accurate numerical fluxes for the temperature and concentration fields which guarantee the sharp treatment of the boundary conditions at the moving front, especially the jump of the concentration according to the liquidus-solidus diagram. We provide some numerical illustrations which assess the good behaviour of the method : maximum principle, stability under CLF condition, numerical convergence toward self-similar solutions, ability to handle two melting fronts.

CONTENTS

1. INTRODUCTION

In the last decades considerable research has been devoted to the simulation of liquid-solid phase change, which is of major importance in several industrial applications, for instance in metallurgical engineering [1, 5, 23], but also in the comprehension of complex natural phenomena, for example the melting of icy moons orbiting giant planets [17, 13, 21]. Such problems are characterized by a moving interface separating the liquid and the solid phases. When the material is pure, the interface is at a constant melting temperature and its motion is defined by a Rankine–Hugoniot type jump relation of the heat fluxes at the melting free boundary [1, 22]. This configuration, known as the two-phase Stefan problem, has been the subject of a huge literature, from modelling and analysis to numerics, see

2010 *Mathematics Subject Classification.* 80A22, 65M08, 80M12.
Key words and phrases. Binary alloy, solidification, sharp model, Stefan problem, finite volume method, Lagrange projection scheme, random sampling projection.

[9, 15, 16, 18] and [19] for ar review. When a solute is present in the material, the phase transition is then driven by a coupled heat and mass transfer process. It induces a jump in concentration at the melting front while the temperature remains continuous. The interface is at the melting temperature which is no longer constant but depends on the concentration of the solute on the both sides of the melting free boundary. The temperature is defined by the so-called liquidus–solidus phase diagram, that is the equilibrium phase diagram of the mixture which prescribes the temperature of the interface as a function of the concentrations of the solute in the liquid and the solid phases that can coexist at thermodynamical equilibrium. Far from the melting front, the problem is modelled by phasic heat and mass diffusion equations given by the Fourier and the Fick laws. This formulation, often called the Rubinstein's model, has been studied, among other references, in the works of Rubinstein [16], Alexiades, Solomon and Wilson [26, 1], Voller and co-authors [23, 24, 25], Visintin [22]. When appropriate initial and boundary conditions are considered, the one-dimensional model admits an analytical self-similar solution as soon as the liquidus-solidus diagram has a linear shape [1]. We refer also to [19] for a condensed summary of the properties and self-similar solutions of the Rubinstein and Stefan-like models. While enriching the model by cross effect terms between heat and mass diffusion, it is possible to exhibit properties of parabolicity and maximum principle. In [22], Visintin points out the importance of these cross effects terms which allow to prove the existence of weak solutions in several space dimension. Note that, in the latter two references, the authors assume the occurence of a mushy region, leading to a diffuse interface between the liquid and the solid phases, and, in turn to a continuum concentration field. However, the applications we have in mind come from the study of the hydrospheres of icy moons of the solar system. Hence the characteristic length scale of the melting front is much smaller than the characteristic length scale of the domain. Therefore it imposes a sharp description of the melting boundary where the concentration is discontinuous across the solidification front whereas the temperature remains continuous. For that purpose, we will focus on the original sharp moving front model proposed by Rubinstein [16] and provide a sharp numerical treatment of the boundary constraints imposed at the interface.

As far as numerics is concerned, several methods have been proposed, initially defined for Stefan-type problems and adapted to the coupling with mass diffusion. The most popular methods are implicit in the sense that they do not rely on an explicit representation of the interface. Some of these methods rely on diffuse interface approximation and the appearance of a mushy region. For sake of completeness we give also some insights of *diffuse* methods even if we focus on *sharp* interface methods.

The enthalpy method consists in the evaluation of the latent heat to track the moving front. The evolution of the latent heat is governed by the enthalpy (or energy) conservation law and the enthalpy function is defined as a piecewise linear function of the temperature. The jump of enthalpy at the front is due to the heat released or absorbed during the solidification process. The works of Voller and coauthors give a good understanding of the method, see for instance [23, 24, 25]. Based on a finite difference formulation, the method turns to be well-suited for diffuse interface model and/or micro-scale description of the interface, but require high order approximations to deal with sharp interface model [24]. Another well-known approach, called phase-field method, consists in a reformulation of the problem: the domain is parametrized by a phase field function which is a fixed constant in each phase and varies smoothly within 0 and 1 in the diffuse interface region. The

thickness of the interface is an artificial parameter of the problem and it is mandatory to provide both a phase-field model and a numerical scheme which converge to the sharp model interface as the thickness parameter goes to zero. The question of convergence is adressed for instance in [5] (see also [11] for the numerical aspects). The drawback of the method is that the discretization parameter has to be much smaller than the thickness parameter leading to a CPU consuming method to recover a sharp interface discretization.

The level set method are very popular for the tracking of sharp interface. It relies on the definition of a level set function whose zero indicates the front position. This function satisfies an additional transport equation, and the diversity of the methods relies on the definition of this velocity. It also requires several regularization steps which lead to a complex algorithm. There exists a large literature on this topic, see for instance [9] and related works in the case of the two-phase Stefan problem, and more recently, [20] for the Rubinstein's model. Note that these references propose finite differences approximation on cartesian grids. An extension of the method is possible on unstructured meshes, see for instance [4, 10] for recent developments in this direction.

We propose in this paper to adapt a Lagrange-projection method with random sampling projection for the Stefan-like problems. The technique has been initially developed for hyperbolic problems which exhibit sharp discontinuities: in [7] for nonconservative hyperbolic problems for compressible materials, in [8] for traffic flow models, in [2] for compressible fluid-particule interaction or in [3, 14] for the simulation of two-fluid flows. In the Lagrangian step, the mesh cells adjacent to the phase boundary are modified by its deplacement. On both sides of the boundary, the diffusion equations of the temperature and the concentration are solved by an explicit in time finite volume scheme within each phase. In order to come back to the original mesh, we make use of a random sampling for projecting the moving front at an interface of the original mesh. This technique avoids dealing with moving mesh and, since it is similar to Glimm scheme method [12], it possesses statistically conservation properties (see [14]).

The outline of the paper is as follow. Section 2 begins by an introduction to the equilibrium thermodynamics of the binary alloy. Then we state the governing equations of the melting problem and recall some properties of the model (existence of weak solutions, similarity solution in 1D, parabolicity, maximum principle). In Section 3 we present the Lagrange-remap method. We first depict the Lagrangian step and the explicit finite volume scheme. Due to the constraints imposed at the moving front, a special attention will be paid to the design of accurate numerical fluxes for the temperature and the concentration fields in the Lagrangian step. At the moving front, the Stefan condition imposes that the interface velocity is proportional to the jump of gradient of temperature, so that the numerical fluxes for the temperature field at the moving front must express this lake of conservation. Conversely the diffusion of the concentration is conservative across the moving front, leading to a jump of the concentration according to the liquidus-solidus diagram. We prove that the Lagrangian step is stable under CFL conditions and ensures the maximum principle. We emphasize that the numerical fluxes for the concentration field at the moving front are consistent with the equilibrium phase diagram and do not require the use of linear liquidus and solidus curves but are adapted to general non-eutectic diagrams. The Section ends with a detailed algorithm of the random projection step. Section 4 is devoted to numerical illustrations. Our method is compared to a level set approach on a classical two-phase Stefan test case. Then we compared our method to an exact solution of the Rubinstein's model when the

liquidus-solidus curves are linear. The Section ends with a non-standard test case with two moving melting fronts obeying different liquidus-solidus diagrams.

2. A sharp interface binary mixture model

This Section concerns the modelling of a mixture of two components A and B, that are soluble in each other, submitted to solidification or melting. We introduce a model of one free moving boundary problem. Taking into account the concentration of the component B in the solvent A, the model boils down to a Stefan-like problem with thermodynamical constraints at the moving interface. We first describe the equilibrium thermodynamics of a binary alloy by means of liquidus-solidus diagram. Then we introduce Stefan-like model. Rewritting the model with a singular source term allows to get rid of the free moving formulation and consider several interfaces.

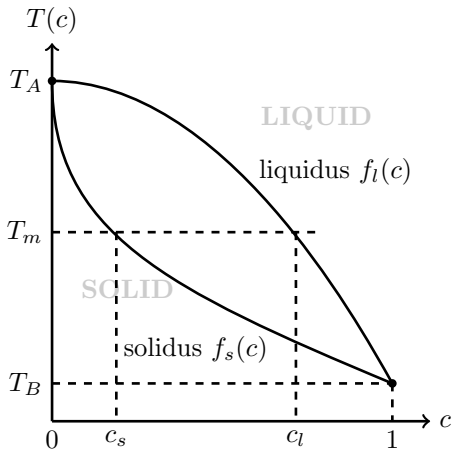

FIGURE 1. Phase diagram of the binary mixture

2.1. **Equilibrium thermodynamics of a binary alloy.** Consider a mixture of two components A and B that are soluble in each other. We assume that the components are intermixed on the atomic length-scale and that the mixture has a constant density ρ. Let T be the temperature of the mixture and $c \in [0,1]$ be the concentration of the component B in the solvent A. The mixture can be either in its solid phase (with index s) or its liquid phase (with index l). The components A and B are characterized by their melting temperature T_A and T_B respectively. An interesting feature of this physical problem is that the concentration c admits a jump from one phase to the other while the temperature remains continuous. One can give a good representation of this phenomenon using an equilibrium phase diagram in the (c,T) plane as the one sketched in Figure 1. The upper curve, called the liquidus line, corresponds to the freezing temperature of the liquid phase depending on the concentration c and is given by the function $f_l : c \in [0,1] \mapsto T \in [T_A, T_B]$. The lower curve is the solidus line defined by the function $f_s : c \in [0,1] \mapsto T \in [T_A, T_B]$ and represents the melting temperature of the solid phase depending on the concentration. In the sequel we adopt the following assumptions.

Assumptions 2.1. *The functions $f_k : c \in [0,1] \mapsto T \in [T_A, T_B]$, $k = l, s$, are such that*

- *$f_s(0) = f_l(0) = T_A$ and $f_s(1) = f_l(1) = T_B$,*
- *f_s and f_l are strictly increasing or decreasing functions of the concentration,*

- *there exists no concentration* $\bar{c} \in]0,1[$ *such that* $f_s(\bar{c}) = f_l(\bar{c})$, *i.e. we restrict ourselves to noneutectic composite.*

These assumptions are useful for theoretical and numerical considerations and will be discussed in Section 3.1.

At the temperature $T_B < T_m < T_A$ the liquidus curve (resp. solidus curve) intersects the line $T = T_m$ at the point c_l (resp. c_s). Hence at thermodynamical equilibrium the interface has to be at the equilibrium temperature T_m to exhibit the concentrations c_l in the liquid phase and c_s in the solid phase. The concentration is thus a piecewise constant function with a jump between c_l and c_s at the melting front.

Note that in numerous paper the authors define the zone between the liquidus and the solidus lines as a mushy region. The reader will find comments on the occurence of a mushy region in [1], see also [25, 24] for numerical purposes. This interpretation leads to a diffuse interface model description. However, for the applications we have in mind, we will focus on the sharp moving interface problem without appearance of any mushy region.

2.2. **A sharp moving interface model.** We focus here on a one moving boundary problem. Assume the binary alloy occupies an one-dimensional open domain $\Omega = [0, +\infty[$, separated into a solid and a liquid zones. Without loss of generality, we set the solid zone in the left side of the domain, that is $\Omega_s(t) := \{(t,x) | t > 0, x < s(t)\}$ and the liquid zone in the right part with $\Omega_l(t) := \{(t,x) | t > 0, s(t) < x\}$. The point separating the solid and the liquid phases determines the position $s(t)$ of the interface in time, initially located in $s(0) = s_0$, which evolves in space and time with velocity $\dot{s}(t)$. We assume that $(0) = s_0 \neq 0$.

The model consists in diffusion equations on the temperature T and on the concentration c which are deduced from the energy conservation and the Fourier's law together with the mass conservation principle and the Fick's law. The model reads

$$\rho \partial_t (c_{p,s} T)(t,x) - \partial_x (K_s \partial_x T)(t,x) = 0, \quad \text{for } (t,x) \in \Omega_s(t), \tag{1}$$

$$\partial_t c(t,x) - \partial_x (D_s \partial_x c)(t,x) = 0, \quad \text{for } (t,x) \in \Omega_s(t), \tag{2}$$

$$\rho \partial_t (c_{p,l} T)(t,x) - \partial_x (K_l \partial_x T)(t,x) = 0, \quad \text{for } (t,x) \in \Omega_l(t), \tag{3}$$

$$\partial_t c(t,x) - \partial_x (D_l \partial_x c)(t,x) = 0, \quad \text{for } (t,x) \in \Omega_l(t), \tag{4}$$

$$\rho L \dot{s}(t) = K_s \partial_x T(t, s(t)^-) - K_l \partial_x T(t, s(t)^+), \tag{5}$$

$$\dot{s}(t)(c(t, s(t))^+ - c(t, s(t)^-)) = D_s \partial_x c(t, s(t)^-) - D_l \partial_x c(t, s(t)^+), \tag{6}$$

$$T(t, s(t)) = T_m(t) = f_s(c(t, s(t)^-)) = f_l(c(t, s(t)^+)), \tag{7}$$

where $s(t)^-$ denotes the left limit $x \to s(t)$ with $x < s(t)$ (*i.e.* in the solid phase) and $s(t)^+$ is the right limit $x \to s(t)$ with $x > s(t)$ (*i.e.* in the liquid phase). Equations (1)-(4) are the phasic diffusion equations where ρ is the constant density of the mixture, $c_{p,k}$ is the specific heat of the phase $k = l, s$ $[Jkg^{-1}K^{-1}]$, K_k is the thermal conductivity $[Wm^{-1}K^{-1}]$, D_k is the mass diffusivity $[m^2 s^{-1}]$. The equation (5) is the so-called Stefan condition which defines the front velocity as the jump of heat flux at the interface, with L the latent heat of solidification $[Jkg^{-1}]$. We assume the parameters $L, K_k, C_{p,k}$ and D_k to be positive constants in each phase $k = l, s$ and do not depend on the temperature nor on the concentration. The interface equation (6) expresses the jump of concentration at the interface while equation (7) imposes the continuity of the temperature at the interface which is given by the liquidus-solidus equilibrium.

The model is endowed with the following initial conditions

$$\begin{aligned} &s(0) = s_0 \neq 0, \quad c(0,x) = c_i(x) \in [0,1], \text{for } x \in \Omega \\ &T(0,x) = \begin{cases} T_{i,s} < T_A, & \text{if } x < s_0, \\ T_{i,l} \geq f_l(c_i(x)), & \text{if } x > s_0, \end{cases} \end{aligned} \tag{8}$$

and we consider in the sequel the following boundary conditions for the temperature and concentration fields

$$\begin{aligned} &T(t,0) = T_{i,s} < T_A, \quad \partial_x T(t,x) = 0 \text{ for } x \to +\infty, \\ &\partial_x c(t,x) = 0 \text{ for } x \to +\infty \text{ and } x = 0. \end{aligned} \tag{9}$$

We now state some properties of the model. We refer to the given references for the detailed proofs.

According to [1] and [19], the one-dimensional system (1)-(7) is parabolic and preserves the positivity of the temperature T and a concentration c between 0 and 1. Furthermore, when endowed with conditions (8) and (9) and with particular choice of liquidus-solidus diagram, it admits a self-similar solution, for which the concentration in the solid phase is constant, the temperature and the concentration in the liquid phase are error functions of the self-similar variable $x/\sqrt{t}$ and the interface position $s(t)$ is proportional to $\sqrt{t}$. In Section 4.2, we provide a particular self-similar solution of (1)-(7) with modified initial boundary conditions.

The model (1)-(7) does not account for cross effect terms between heat and mass diffusion: a mass flux should be induced by the temperature gradient (this is the Soret effect) and a heat flux should be caused by the mass transfer (known as the Dufour effect). In [1], the authors enhance these terms to the multi-dimensional system and prove its parabolicity under condition. Moreover, according to [22], these terms are mandatory to prove the existence of a weak solution to the multi-dimensional system. Note that this terms are not quantitatively significant, especially in one-dimension, that's why we choose to get rid of them.

An interesting feature of the moving boundary model (1)-(7) is that it can be written under the following equivalent condensed form, for $t > 0, x \in \Omega$,

$$\rho \partial_t (c_p T) - \partial_x (K \partial_x T) = -\left(\rho L + \rho T_m (c_{p,s} - c_{p,l})\right) \dot{s}(t) \delta_0 (x - s(t)), \tag{10}$$

$$\partial_t c - \partial_x (D \partial_x c) = 0, \tag{11}$$

together with the interface condition (7) and introducing the piecewise constant functions

$$(c_p, K, D) = (c_{p,s}, K_s, D_s) \mathbf{1}_{0 \leq x < s(t)} + (c_{p,l}, K_l, D_l) \mathbf{1}_{x > s(t)}. \tag{12}$$

The notation $\delta_0(.)$ stands for the Dirac mass so that the source term in the first equation is isolated and active only at the interface $s(t)$. Computing Rankine-Hugoniot relations for (10)-(11) at the interface $s(t)$ leads to

$$\begin{aligned} \dot{s}(t) \rho \left[c_{p,l} T(t, s(t)^+) - c_{p,s} T(t, s(t)^-) \right] = &-K_l \partial_x T(t, s(t)^+) + K_s \partial_x T(t, s(t)^-) \\ &- \left(\rho L + \rho T_m (c_{p,s} - c_{p,l})\right) \dot{s}(t), \end{aligned} \tag{13}$$

$$\dot{s}(t) \left[c(t, s(t)^+) - c(t, s(t)^-) \right] = -D_l \partial_x c(t, s(t)^+) + D_s \partial_x c(t, s(t)^-). \tag{14}$$

Thanks to the liquidus-solidus equilibrium (7), the jump relation (13) boils down to the Stefan condition (5), while (14) complies with the relation (6). Hence the interface constraints are implicitly contained in the condensed model (7)-(10)-(11). Note that the computation of the interface constraints by means of Rankine-Hugoniot relations has been conducted in numerous works, see for instance [22] and [1]. The singular source term formulation allows to get rid of the implicit definition of the interface like for free boundaries problem formulation. Moreover the heat and mass

equations are now stated in the whole domain Ω without distinguishing the liquid and the solid zones. It enables to handle several moving fronts in a simpler manner.

3. Random choice interface capturing method

We now turn to the approximation of the reformulated model (10)-(11)-(7). We adapt the Lagrange-projection method with random sampling remap developed in [6] for the computation of nonclassical shocks of scalar conservation laws, in [8] for traffic flow model, in [2] for the interaction of a solid particule with a compressible fluid and in [3, 14] for the interface tracking in a compressible two-phase flow. The method consists in two steps. In a first step we use a finite volume approximation of the temperature and the concentration fields with appropriate numerical fluxes. Since the singular source term is only active at the interface, the temperature and the concentration equations are conservative far from the interface. Hence we consider classical conservative numerical fluxes in the solid and liquid domains. A special attention is paid to the definition of the numerical fluxes at the melting front in order to be consistent with the interface constraints (5) and (7). First a notable feature is the shape of the space-time cells on both side of the interface. Since the melting interface is moving, the neighbouring space-time cells of the interface are trapezoidal (see Figure 2). This leads to a particular definition of the finite volume scheme in these two cells. Second the difference between the temperature fluxes at the moving interface corresponds to the lake of conservation due to the singular source term (see (10)). Hence we design in Section 3.1.1 a well-balanced scheme for the temperature. The numerical scheme admits good properties (continuity of the temperature at the interface, positivity). Then we build the numerical flux for the concentration in Section 3.1.2. It complies with the conservation form of the concentration equation (see (11)) and guarantees the jump of the concentration according to general noneutectic liquidus-solidus diagram, following Figure 1. Again the finite volume scheme accounts for the trapezoidal shape of the space-time cells on both side of the moving interface. We emphasize that we consider an explicit time-discretization (comments on implicit integration are given in conclusion).

The second step consists in a remap stage: the front is placed at a grid interface at each time step by mean of random sampling. This avoids the use of a moving mesh which makes the method easier to implement. In Section 3.2 we provide the algorithm of the random projection step. The projection is active at the moving front only which implies that the scheme is statistically conservative (we refer to [3] for numerical illustrations and [14] for a detailed proof).

3.1. Lagrangian step and numerical fluxes.

We consider a uniform mesh of the one-dimensional domain Ω with cells $C_i = [x_{i-1/2}, x_{i+1/2}[$, centered in $x_i = i\Delta x$, $i \in \mathbb{Z}$. The computational domain is assumed to be infinite to avoid difficulties due to boundary conditions (the questions of boundary conditions will be adressed in the next section depending on the considered test case). We denote by Δt the time step and by T_i^n and c_i^n a constant per cell approximation of the temperature T and the concentration c at time $t^n = n\Delta t$ within the cell C_i. Let s^n be the position of the moving front at time t^n, and assume that it coincides with the grid interface $s^n = x_{1/2}$. At this stage, we assume that the front evolves with the constant velocity v between t^n and t^{n+1}, such that, before the random projection step, its position at time t^{n+1} is $\tilde{s}^{n+1} = x_{1/2} + v\Delta t$. To avoid the disappearance of a cell, we classically impose

$$|v| \leq \frac{\Delta x}{\Delta t}. \tag{15}$$

Since $s^n = x_{1/2}$, the cells C_i with $i \leq 0$ (resp. $i \geq 1$) belong to the solid domain Ω_s (resp. the liquid domain Ω_l).

The purpose of the lagrangian step is to compute the approximated temperature and concentration field $\tilde{T}_i^{n+1}, \tilde{c}_i^{n+1}$ within the cell C_i, $i \in \mathbb{Z}$, using a finite volume approximation and appropriate numerical fluxes at the grid interfaces. Since the temperature and the concentration have different behaviour at the moving front and since the equations (10)-(11) are coupled solely by the singular source term and the constraint (7), we can distinguish the construction of the numerical fluxes of the temperature from those of the concentration.

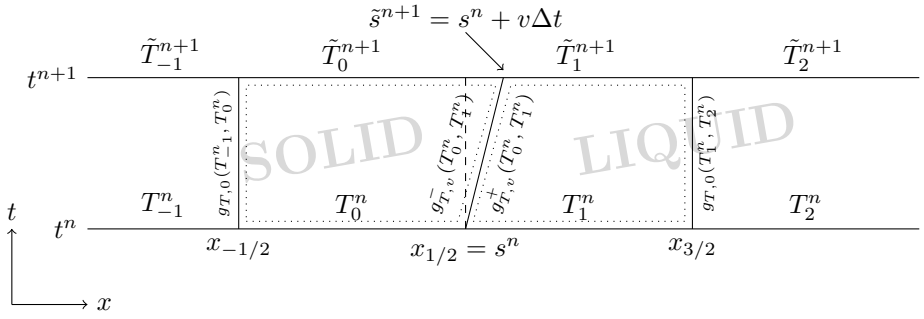

FIGURE 2. Lagrangian step for the temperature field. Far from the moving front, a classical monotone numerical flux $g_{T,0}$ is used. At the interface one uses the numerical fluxes $g_{T,v}^-$ and $g_{T,v}^+$ (see (37)) which take into account the singular source term in equation (10).

3.1.1. *Numerical fluxes for the temperature.* We focus on the discretization of the heat equation

$$\begin{cases} \rho\partial_t(c_pT) - \partial_x(K\partial_xT) = -\rho(L + T_m(c_{p,s} - c_{p,l})\dot{s}(t))\delta_0(x - s(t)), \\ \qquad\qquad\qquad\qquad\qquad\qquad\qquad\qquad t \in [t^n, t^{n+1}[,\ x \in \Omega, \\ T(t^n, x) = \sum_{i\in\mathbb{Z}} T_i^n \mathbf{1}_{[x_{i-1/2}, x_{i+1/2}[}, \\ s(t^n) = x_{1/2}, \\ T(t^n, s(t^n)) = T_m, \\ \dot{s}(t) = v, \forall t > 0, \end{cases} \tag{16}$$

between time t^n and t^{n+1}, where the interface temperature T_m and velocity $v \in \mathbb{R}$ are given and the coefficient c_p and K admit a jump at the interface following (12).

Far from the moving front, the finite volume formulation corresponds to the integration of the heat equation (16) on the space-time rectangle $C_i \times (t^n, t^{n+1})$ (see Figure 2). It yields for all $i \neq 0, 1$

$$\tilde{T}_i^{n+1} = T_i^n - \frac{\Delta t}{\Delta x}(g_{T,0}(T_i^n, T_{i+1}^n) - g_{T,0}(T_{i-1}^n, T_i^n)), \tag{17}$$

where the numerical flux $g_{T,0}$ is consistent with the heat flux $-K_k/(\rho c_{p,k})\partial_xT$ within the phasic subdomain Ω_k, $k = l, s$. In practice we consider the first order approximation

$$g_{T,0}(T_i^n, T_{i+1}^n) = -K_i/(\rho c_{p,i})\frac{T_{i+1}^n - T_i^n}{\Delta x}, \quad i \neq 0, 1. \tag{18}$$

We now focus on the definition of finite volume scheme near the moving front. The integration of the heat equation (16) on the space-time trapezoid $(x_{-1/2}, t^n) -$

$(x_{1/2}, t^n) - (x_{1/2} + v\Delta t, t^{n+1}) - (x_{-1/2}, t^{n+1})$ (see Figure 2) leads to the following approximation of the temperature

$$(\Delta x + v\Delta t)\tilde{T}_0^{n+1} = \Delta x T_0^n - \Delta t(g^-_{T,v}(T_0^n, T_1^n) - g_{T,0}(T_{-1}^n, T_0^n)), \tag{19}$$

where the flux $g_{T,0}(.,.)$ is classically defined by (18) whereas the flux $g^-_{T,v}(T_0^n, T_1^n)$ has to be consistent with the lagrangian heat flux $-K_s/(\rho c_{p,s})\partial_x T - vT$ at the moving front. Similarly the integration of the heat equation on the space-time trapezoid $(x_{1/2}, t^n) - (x_{3/2}, t^n) - (x_{3/2}, t^{n+1}) - (x_{1/2} + v\Delta t, t^{n+1})$ gives

$$(\Delta x - v\Delta t)\tilde{T}_1^{n+1} = \Delta x T_1^n - \Delta t(g_{T,0}(T_1^n, T_2^n) - g^+_{T,v}(T_0^n, T_1^n)), \tag{20}$$

where $g_{T,0}$ is again given by (18) and $g^+_{T,v}(T_0^n, T_1^n)$ must be consistent with the lagrangian flux$-K_l/(\rho c_{p,l})\partial_x T - vT$ at the moving front. We consider the following numerical fluxes

$$\begin{aligned} g^-_{T,v}(T_0, T_1) &= -\frac{K_s}{\rho c_{p,s}} \frac{T_m - T_0}{\Delta x/2} - vP^-(x_{1/2} + v\Delta t/2), \\ g^+_{T,v}(T_0, T_1) &= -\frac{K_l}{\rho c_{p,l}} \frac{T_1 - T_m}{\Delta x/2} - vP^+(x_{1/2} + v\Delta t/2), \end{aligned} \tag{21}$$

with

$$P^-(x) = \frac{T_1^n - T_m}{\Delta x/2}(x - x_{1/2}) + T_m, \quad P^+(x) = \frac{T_m - T_0^n}{\Delta x/2}(x - x_0) + T_0^n. \tag{22}$$

The function P^+ (resp. P^-) is a first order Lagrange polynomial defined by the points (x_0, T_0^n) (resp. (x_1, T_1)) and $(x_{1/2}, T_m)$, such that $P^\pm(x_{1/2} + v\Delta t/2)$ corresponds to a first order approximation of the temperature at the point $x_{1/2} + v\Delta t/2$ and ensures $P^\pm(x_{1/2}) = T_m$.

Proposition 3.1. *Consider a datum $(T_i^n)_{i\in\mathbb{Z}}$ such that $T_i^n \geq 0$, $\forall i \in \mathbb{Z}$. Under the stability condition*

$$\Delta t \leq \Delta x^2/(3\min(\alpha_l, \alpha_s)), \tag{23}$$

with $\alpha_k = K_k/(\rho c_{p,k})$, $k = l, s$, the scheme (17)-(22) guarantees the positivity of the temperature, i.e. $\tilde{T}_i^{n+1} \geq 0$, $\forall i \in \mathbb{Z}$.

Moreover, suppose $c_{p,s} = c_{p,l}$ and $K_s = K_l$ and consider a initial datum $T_i^n = \frac{1}{\Delta x}\int_{C_i^n} \beta x\, dx$ with $\beta \in \mathbb{R}$ and fix $T_m = \beta x_{1/2}$. Then, the scheme exactly preserves the initial linear profile, i.e. $\tilde{T}_i^{n+1} = \frac{1}{\Delta x}\int_{\tilde{C}_i^{n+1}} \beta x\, dx$, $\forall i \in \mathbb{Z}$.

Proof. Positivity. The positivity is a consequence of the monotonicity of the scheme (17)-(22). For $i < 0 \in \mathbb{Z}$, the scheme reads

$$\begin{aligned} \tilde{T}_i^{n+1} &= T_i^n(1 - 2\alpha_i\Delta t/\Delta x^2) + (T_{i+1}^n + T_{i-1}^n)\alpha_i\Delta t/\Delta x^2 \\ &=: \mathcal{F}(T_{i-1}^n, T_i^n, T_{i+1}^n). \end{aligned} \tag{24}$$

The function $\mathcal{F}$ is nondecreasing with respect to its three arguments if $\Delta t \leq \Delta x^2/(2\alpha_s)$. Moreover $\mathcal{F}(0,0,0) = 0$. Hence $\tilde{T}_i^{n+1} \geq 0$. The same construction holds in the liquid domain with the condition $\Delta t \leq \Delta x^2/(2\alpha_l)$. Focus now on the cell $i = 0$. One has

$$\begin{aligned} (\Delta x + v\Delta t)\tilde{T}_0^{n+1} &= T_0^n(\Delta x - 3\alpha_s\Delta t/\Delta x) + T_1^n v^2\Delta t^2/\Delta x + T_{-1}^n\alpha_s\Delta t/\Delta x \\ &\quad + T_m\Delta t/\Delta x(2\alpha_s - v(v\Delta t - \Delta x)) \\ &=: \mathcal{F}_0(T_{-1}^n, T_0^n, T_1^n). \end{aligned} \tag{25}$$

One observes that the function $\mathcal{F}_0$ is nondecreasing with respect to its three arguments if $\Delta t \leq \Delta x^2/(3\alpha_s)$ and satisfies $\mathcal{F}_0(0,0,0) = 0$. The same holds for $i = 1$

with a function $\mathcal{F}_1(T_0^n, T_1^n, T_2^n)$ which is nondecreasing if $\Delta t \leq \Delta x^2/(3\alpha_l)$ and satisfies $\mathcal{F}_1(0,0,0) = 0$. Hence, denoting

$$T_\Delta(t,x) = \sum_{n\in\mathbb{N}} \sum_{i\in\mathbb{Z}} T_i^n \mathbf{1}_{[n\Delta t,(n+1)\Delta t[\times C_i}(t,x),$$

one has $0 \leq T_\Delta(t,x)$ for a.e. $t > 0$ and $x \in \mathbb{R}$ as soon as (23) is fulfilled.

Preservation of stationary solutions. Far from the interface, the consistency of the numerical flux $g_{T,0}$ implies that $\tilde{T}_i^1 = \beta x_i$, $\forall i \neq 0, 1$. We now focus on the cell C_0. At time t^1, the cell C_0 becomes $[x_{-1/2}, x_{1/2} + v\Delta t]$. Furthermore the numerical scheme (19) with the initial datum gives

$$(\Delta x + v\Delta t)\tilde{T}_0^1 = (\Delta x + v\Delta t)\beta(x_0 + v\Delta t/2) = \int_{x_{-1/2}}^{x_{1/2}+v\Delta t} \beta x\, dx.$$

Hence the linear profile is preserved on the moving cell C_0. The same property holds in the cell C_1 which coincides, at time t^1, with $[x_{1/2} + v\Delta t, x_{3/2}]$ since the scheme (20) gives

$$(\Delta x - v\Delta t)\tilde{T}_1^1 = \int_{x_{1/2}+v\Delta t}^{x_{3/2}} \beta x dx.$$

By induction the scheme preserves stationnary profiles for any $n \geq 1$. □

3.1.2. *Numerical flux for the concentration.* We now turn to the finite volume approximation of the mass diffusion

$$\begin{cases} \partial_t c - \partial_x(D\partial_x c) = 0,\ t \in [t^n, t^{n+1}[, x \in \Omega, \\ c(t^n, x) = \sum_{i\in\mathbb{Z}} c_i^n \mathbf{1}_{[x_{i-1/2}, x_{i+1/2}[}, \\ s(t^n) = x_{1/2}, \\ \dot{s}(t) = v,\ \forall t > 0, \\ c(t^n, s(t^n)^-) \neq c(t^n, s(t^n)^+), \\ f_s(c(t^n, s(t^n)^-)) = f_l(c(t^n, s(t^n)^+)), \end{cases} \tag{26}$$

between times t^n and t^{n+1} where the diffusion coefficient D admits a jump at the interface following (12). Far from the moving front, the integration of the mass diffusion on the rectangle $C_i \times (t^n, t^{n+1})$ leads to the following finite volume formulation for all $i \neq 0, 1$

$$\tilde{c}_i^{n+1} = c_i^n - \frac{\Delta t}{\Delta x}(g_{c,0}(c_i^n, c_{i+1}^n) - g_{c,0}(c_{i-1}^n, c_i^n)), \tag{27}$$

where the numerical flux $g_{c,0}$ is consistent with the mass flux $-D\partial_x c$.

Like for the temperature field, we choose the first order approximation

$$g_{c,0}(c_i^n, c_{i+1}^n) = -D_i \frac{c_{i+1}^n - c_i^n}{\Delta x}. \tag{28}$$

Near the moving front the numerical scheme has to guarantee the jump of the concentration at the front and the liquidus-solidus constraint $f_s(c(t, s(t)^-)) = f_l(c(t, s(t)^+))$. We introduce the numerical flux $g_{c,v}^\star$ which is consistent with the lagrangian flux at the interface $-D\partial_x c - vc$ and copes with the conservation of the concentration equation. The scheme writes

$$\begin{aligned} (\Delta x + v\Delta t)\tilde{c}_0^{n+1} &= \Delta x c_0^n - \Delta t(g_{c,v}^\star(c_0^n, c_1^n) - g_{c,0}(c_{-1}^n, c_0^n)), \\ (\Delta x - v\Delta t)\tilde{c}_1^{n+1} &= \Delta x c_1^n - \Delta t(g_{c,0}(c_1^n, c_2^n) - g_{c,v}^\star(c_0^n, c_1^n)), \end{aligned} \tag{29}$$

where the numerical flux $g^\star_{c,v}$ is defined by

$$g^\star_{c,v}(c_0^n, c_1^n) = \begin{cases} -D_l \dfrac{c_1^n - \overline{c}}{\Delta x/2} - v\overline{P}(x_{1/2} + v\Delta t/2), & \text{with } \overline{c} \text{ such that } \overline{H}(\overline{c}) = 0, \\ -D_s \dfrac{\underline{c} - c_0^n}{\Delta x/2} - v\underline{P}(x_{1/2} + v\Delta t/2), & \text{with } \underline{c} \text{ such that } \underline{H}(\underline{c}) = 0, \end{cases} \tag{30}$$

where

$$\begin{aligned} \overline{H}(c) &= c(D_l - \frac{v}{2}(\Delta x + v\Delta t)) + f_s^{-1} \circ f_l(c)(D_s + \frac{v}{2}(\Delta x - v\Delta t)) \\ &\quad - c_1^n(D_l - v^2\Delta t/2) - c_0^n(D_s - v^2\Delta t/2), \\ \underline{H}(c) &= f_l^{-1} \circ f_s(c)(D_l - \frac{v}{2}(\Delta x + v\Delta t)) + c(D_s + \frac{v}{2}(\Delta x - v\Delta t)) \\ &\quad - c_1^n(D_l - v^2\Delta t/2) - c_0^n(D_s - v^2\Delta t/2), \end{aligned} \tag{31}$$

and

$$\overline{P}(x) = c_0^n + \frac{\overline{c} - c_0^n}{\Delta x/2}(x - x_0), \quad \underline{P}(x) = \underline{c} + \frac{c_1^n - \underline{c}}{\Delta x/2}(x - x_{1/2}). \tag{32}$$

The quantity $\overline{c}$ is an approximation of the concentration $c(t, s(t)^+)$ while $\underline{c}$ approaches $c(t, s(t)^-)$. The functions $\overline{H}$ and $\underline{H}$ are such that the liquidus-solidus constraint is satisfied at the interface *i.e.* $f_s(\underline{c}) = f_l(\overline{c})$. The definition of the numerical flux strongly relies on the existence of a unique concentration $\overline{c}$ solution of $\overline{H}(\overline{c}) = 0$ (or $\underline{c}$ solution of $\underline{H}(\underline{c}) = 0$).

Proposition 3.2. *Assume that c_1^n and c_0^n belong to $[0,1]$ and that Assumptions 2.1 on the liquidus-solidus diagram hold. Under the stability condition*

$$\Delta t \leq 2\frac{\max(D_s, D_l)}{v^2}, \tag{33}$$

then there exist a unique $\overline{c}$ solution of $\overline{H}(x) = 0$ and an unique $\underline{c}$ solution of $\underline{H}(x) = 0$. Furthermore $\overline{c}$ and $\underline{c}$ belong to $[0,1]$.

Proof. The function $\overline{H}$ is strictly increasing as soon as (33) holds. Then observe that $\bar{H}(0) = -D_l c_1^n - D_s c_0^n \leq 0$ and that $\bar{H}(1) = D_l(1 - c_1^n) + D_s(1 - c_0^n) \geq 0$. Thus according to the intermediate value theorem, there exists an unique concentration $\bar{c}$ such that $H(\bar{c}) = 0$. The same arguments hold for $\underline{H}$. □

Note that the scheme guarantees both the jump condition (6) and the liquidus-solidus constraint (7) by construction.

Proposition 3.3. *Let $(c_i^0)_{i\in\mathbb{Z}}$ such that $0 \leq c_i^0 \leq 1$, $\forall i \in \mathbb{N}$. Assume the stability conditions*

$$\Delta t \leq \frac{\Delta x^2}{3\min(D_l, D_s)} \tag{34}$$

and (33) hold. Then the scheme (27)-(31) guarantees $0 \leq \tilde{c}_i^{n+1} \leq 1, \forall i \in \mathbb{Z}$.

Proof. As in the case of temperature, the positivity is a consequence of the monotonicity of the scheme. For $i \in \mathbb{Z}$, $i \neq 1, 0$, the scheme reads

$$\begin{aligned} \tilde{c}_i^{n+1} &= c_i^n(1 - 2D_i\Delta t/\Delta x^2) + (c_{i+1}^n + c_{i-1}^n)D_i\Delta t/\Delta x^2 \\ &=: \mathcal{F}(c_{i-1}^n, c_i^n, c_{i+1}^n). \end{aligned}$$

The function $\mathcal{F}$ is nondecreasing with respect to its three arguments if $\Delta t \leq \Delta x^2/(2D_i)$. Moreover $\mathcal{F}(0,0,0) = 0$ and $\mathcal{F}(1,1,1) = 1$. Then $\tilde{c}_i^{n+1} \in [0,1]$ if

$c_i^n \in [0,1]$. Focus now on the cell $i=0$. According to Proposition 3.2, there exists an unique $\bar{c} \in [0,1]$ such that $\overline{H}(\bar{c}) = 0$. The scheme writes

$$\begin{aligned}(\Delta x + v\Delta t)\tilde{c}_0^{n+1} &= c_0^n(\Delta x - 3D_s\Delta t/\Delta x) + c_{-1}^n D_s \Delta t/\Delta x \\ &\quad + \underline{c}\Delta t(v + 2D_s/\Delta x - v^2\Delta t/\Delta x) \\ &=: \mathcal{F}_0(c_{-1}^n, c_0^n, \underline{c}).\end{aligned}$$

The function $\mathcal{F}_0$ is nondecreasing with respect to its three arguments if $\Delta t \leq \dfrac{\Delta x^2}{3D_s}$ and $\Delta t \leq \dfrac{2D_s}{v^2} + \dfrac{\Delta x}{v}$. The latter condition boils down to the sum of the constraints (15) and (33). Moreover $\mathcal{F}_0(0,0,0) = 0$ and $\mathcal{F}_0(1,1,1) = 1$. Then by a monotonicity argument the scheme is positive. The same arguments hold in the liquid region. □

3.2. **Projection step and general algorithm.** We now turn to the projection step and provide the algorithm for the whole model (10)-(11)-(7).

We denote s^n the position of the interface at time t^n and assume that it coincides with an interface of the mesh. The purpose of the following algorithm is to determine randomly the position s^{n+1} of the interface at time t^{n+1} when it is moving with the speed v^n during the time interval $[t^n, t^{n+1}[$ and to project it on the grid.

The general algorithm is the following.

(1) *Initialization.* Start from $(T_i^n)_{i\in\mathbb{Z}}$, $(c_i^n)_{i\in\mathbb{Z}}$, s^n and v^n which respectively denote the piecewise constant per cell temperature and concentration approximation, the position of the interface and its velocity at time t^n. Assume the interface coincides with a grid interface $s^n = x_{I^n+1/2}$ (see Figure 3).

(2) *Lagrangian step.*
   (a) *Far from the interface s^n.* Compute the approximate temperature $\tilde{T}_i^{n+1}$ and $\tilde{c}_i^{n+1}$ using (17) and (27), $\forall i \neq I^n, I^n+1$.
   (b) *On both sides of the interface s^n.* Compute the approximations $\tilde{c}_{I^n}^{n+1}$ and $\tilde{c}_{I^n+1}^{n+1}$ using (29) and the numerical flux (30)-(31). Compute the approximations $\tilde{T}_{I^n}^{n+1}$ and $\tilde{T}_{I^n+1}^{n+1}$ using (19)-(20) and the numerical fluxes (37)-(22).

(3) Random projection step.
   (a) Build a sequence of pseudo random numbers $y^n \in (0, \Delta x)$ (see details below).
   (b) Project the new interface s^{n+1} depending on the sign of $y^n + v^n\Delta t$ as follow (see Figure 3).
      - If $v^n > 0$, then

$$\begin{cases} (T_{I^n}^{n+1}, c_{I^n}^{n+1}) & = (\tilde{T}_{I^n}^{n+1}, \tilde{c}_{I^n}^{n+1}) \\ (I^{n+1}, T_{I^n+1}^{n+1}, c_{I^n+1}^{n+1}) & = \begin{cases} (I^n+1, \tilde{T}_{I^n}^{n+1}, \tilde{c}_{I^n}^{n+1}) & \text{if } y^n < v^n\Delta t \\ (I^n, \tilde{T}_{I^n+1}^{n+1}, \tilde{c}_{I^n+1}^{n+1}) & \text{else,} \end{cases} \end{cases}$$

      - If $v^n < 0$, then

$$\begin{cases} (I^{n+1}, T_{I^n}^{n+1}, c_{I^n}^{n+1}) = \begin{cases} (I^n, \tilde{T}_{I^n}^{n+1}, \tilde{c}_{I^n}^{n+1}) & \text{if } y^n > -v^n\Delta t \\ (I^n - 1, \tilde{T}_{I^n+1}^{n+1}, \tilde{c}_{I^n+1}^{n+1}) & \text{else,} \end{cases} \\ (T_{I^n+1}^{n+1}, c_{I^n+1}^{n+1}) = (\tilde{T}_{I^n+1}^{n+1}, \tilde{c}_{I^n+1}^{n+1}). \end{cases}$$

   (c) Update the velocity v^{n+1} using the jump relation on the concentration field as follow

$$v^{n+1} = \left(D_l \frac{c_{I^n+1}^n - \overline{c}^n}{\Delta x/2} - D_s \frac{\underline{c}^n - c_{I^n}^n}{\Delta x/2} \right) / (\overline{c}^n - \underline{c}^n), \tag{35}$$

where $\underline{c}^n$ and $\overline{c}^n$ are given by (31).

Let us explain the projection step 3b with help of Figure 3. In Figure 3-top, the random variable satisfies $0 < y^n < v^n \Delta t$, which means that the point $s^n + y$ belongs to the interval of $\tilde{T}_{I^n}^{n+1}$. Hence at time t^{n+1}, the interface is located at $s^{n+1} = I^{n+1} + 1/2 = I^n + 3/2$, that is $I^{n+1} = I^n + 1$, $(T_{I^n}^{n+1}, c_{I^n}^{n+1}) = (\tilde{T}_{I^n}^{n+1}, \tilde{c}_{I^n}^{n+1})$ and $(T_{I^n+1}^{n+1}, c_{I^n+1}^{n+1}) = (\tilde{T}_{I^n}^{n+1}, \tilde{c}_{I^n}^{n+1})$. The converse case $y^n < v^n \Delta t$ is sketched in Figure 3-bottom.

The projection step 3b relies on the definition of the pseudo-random sequence $y^n \in (0, \Delta x)$ in step 3a. In practice we build a the low-discrepancy (k_1, k_2) *van der Corput* sequence computed with relative prime parameters $k_1 = 3 < k_2 = 5$. We refer the reader to [3] and [14] for C algorithm and details the random projection method.

Following [20], the velocity update at step 3c is obtained by mass conservation before sampling) and uses a discrete version the Rankine-Hugoniot condition of the concentration field (6). Note that in the case of the Stefan problem, that is when the concentration field is not taken into account, the velocity is updated using only the Stefan condition (5). In practice, we use

$$\rho L v^{n+1} = (\tilde{g}_{T,v}^{-}(T_{I^n}^n, T_{I^n+1}^n) - \tilde{g}_{T,v}^{+}(T_{I^n}^n, T_{I^n+1}^n)), \tag{36}$$

with

$$\begin{aligned} \tilde{g}_{T,v}^{-}(T_{I^n}^n, T_{I^n+1}^n) &= -K_s \frac{T_m - T_{I^n}^n}{\Delta x/2} - v^n P^-(x_{1/2} + v^n \Delta t/2), \\ \tilde{g}_{T,v}^{+}(T_{I^n}^n, T_{I^n+1}^n) &= -K_l \frac{T_{I^n}^n - T_m}{\Delta x/2} - v^n P^+(x_{1/2} + v^n \Delta t/2), \end{aligned} \tag{37}$$

and the polynomial $P^{\pm}$ defined in (22). Since the numerical fluxes are consistent with the lagrangian heat flux $-K/(\rho c_p)\partial_x T - vT$, the relation (35) is thus consistent with the Stefan condition (5).

Observe that we choose to compute the velocity v^{n+1} explicitly using the numerical fluxes (37) evaluated at time t^n.

4. Numerical results

4.1. **A two-phase Stefan problem.** This first test case consists in the a simple two-phase Stefan problem without mass diffusion nor solidus-liquidus constraint at the interface. Then the model boils down to phasic equations (1)-(3) together with the Stefan condition (5) or equivalently to (10) with $T(t, s(t)) = T_m$. In [15] the authors provide an exact solution for this problem when considering a semi-infinit domain and homogeneous Neumann boundary conditions *i.e.* $\partial_x T(t, x) = 0$, for $x \in \partial\Omega$. For sake of completness we recall the formula provided in [15]. Consider $c_{p,l} = c_{p,s} = \rho = 1$ and the initial piecewise constant temperature profile

$$T(0,x) = \begin{cases} T_l^0, & 0 < x < s(0) \text{ (liquid zone)}, \\ T_m, & x = s(0) \text{ (melting temperature at the interface)}, \\ T_s^0, & s(0) < x \text{ (solid zone)}, \end{cases}$$

the solution reads

$$T(t,x) = \begin{cases} \dfrac{T_l^0(erfc((x - s(0)/2\sqrt{K_l t})) - erfc(\lambda/\sqrt{K_l}))}{2 - erfc(\lambda/\sqrt{K_l})}, & \text{if } x < s(t), \\ T_s^0 - T_s^0 \dfrac{erfc((x - s(0)/2\sqrt{K_s t})}{erfc(\lambda/\sqrt{K_s})}, & \text{if } x > s(t), \\ s(t) = s(0) + 2\lambda\sqrt{t}. \end{cases}$$

The value λ is solution of a non linear equation, which for the set of parameters $L = 0.53$, $K_l = 0.005$, $K_s = 1$, $c_l = c_s = 1 = \rho = 1$, is $\lambda = 0.122595$ (see again

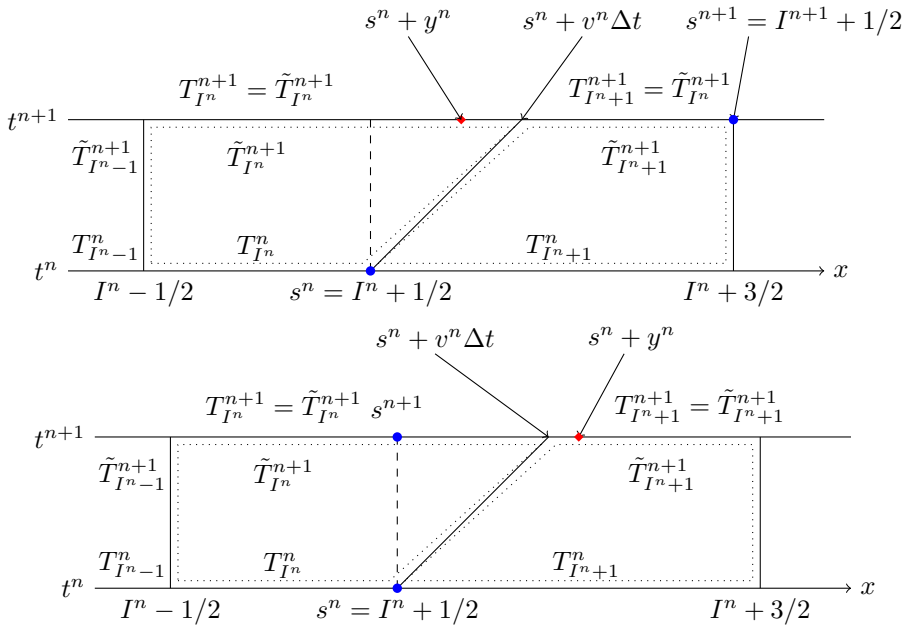

FIGURE 3. Random projection step (for $v^n > 0$). Top: the random variable satisfies $0 < y^n < v^n\Delta t$ (see the red diamond at the left of the moving interface). Then the moving front evolves from $s^n = I^n + 1/2$ to $s^{n+1} = I^{n+1} = I^n + 1$. Bottom: conversely if $\Delta x > y^n > v^n\Delta t$ (see the red diamond at the right of the moving front), then the interface remains fixed from time t^n to t^{n+1}.

[15]). The initial phasic temperatures are $T_s^0 = 0.1$ and $T_l^0 = 0.53$, which means that the solid phase is artificially superheated.

We compare our Random Choice Method (RCM) to the explicit in time level set method developed in [9]. For both numerical methods we consider a uniform mesh of $[0, 5]$ with 2000 cells and a final time $T_{final} = 0.25s$. In Figure 4 one can observe that both numerical method give similar results compared to the exact solution. When zooming on the interface (Figure 4-bottom), one observes that the random sampling method is more precise. When focusing on the position of the interface in time, one can observe on Figure 5-bottom that the Random Choice Method yields a curve with stepped profile. This is due to the random sampling done at each time step at the interface.

4.2. **Rubinstein test case: comparison toward an exact solution.** When considering linear liquidus-solidus diagram, it is possible to compute analytical solutions of the Rubinstein model. Following the proof of [26] (see also similarity solutions listed in the review of Tarzia [18] for numerous Stefan-like problems), we compute a similarity solution as a function of $(x - s_0)/\sqrt{t}$ on the infinite domain $\Omega = \mathbb{R}$. The temperature and the concentration fields satisfy

$$\begin{cases} \lim_{x\to-\infty} T(t,x) = T_{sol}, & \lim_{x\to+\infty} T(t,x) = T_{liq}, \\ \partial_x c(t,x) = 0 \text{ for } x \to \pm\infty, & \lim_{x\to+\infty} c(t,x) = c_{liq}. \end{cases}$$

At the interface, the temperature is assumed to be constant and is given by the liquidus-solidus equilibrium :

$$T(t, s(t)) = T_{int} = f_l(\overline{c}) = f_s(\underline{c}), \tag{38}$$

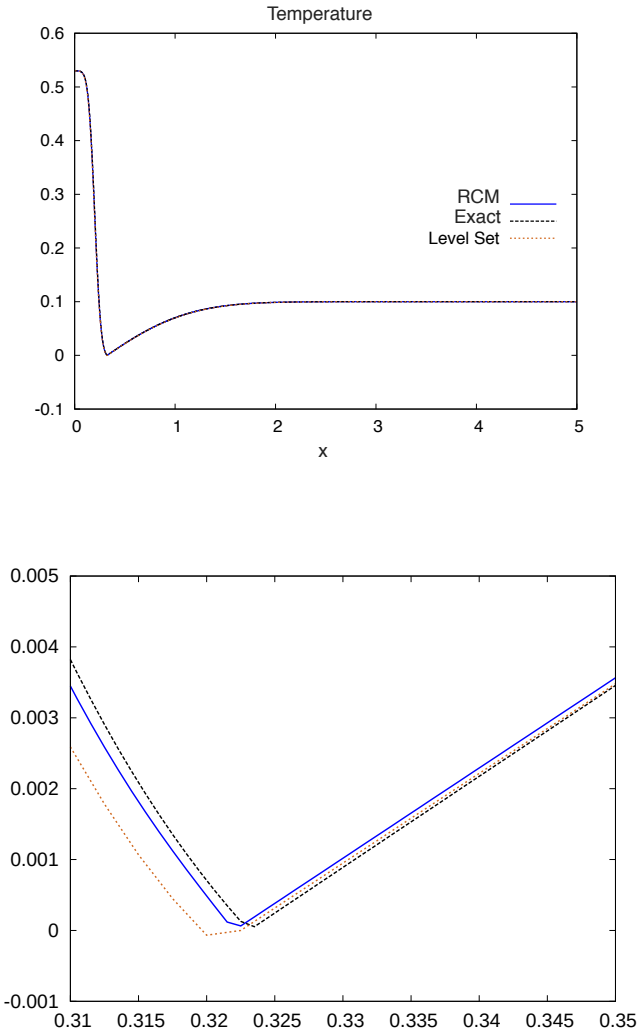

FIGURE 4. Comparison between level set and the random sampling method. Temperature profile in space and a zoom at the interface., position of the interface in time, zoom of the interface position in time.

where $\overline{c} = c(t, s(t)^+)$ and $\underline{c} = c(t, s(t)^-)$. The similarity solution reads

$$T(t,x) = \begin{cases} T_{sol} + \dfrac{T_{int} - T_{sol}}{2 - \operatorname{erfc}\left(\lambda/\sqrt{\alpha_s}\right)} \left(1 + \operatorname{erf}\left(\dfrac{x - s_0}{2\sqrt{\alpha_s t}}\right)\right) & \text{if } x < s(t), \\ T_{liq} + \dfrac{T_{liq} - T_{int}}{\operatorname{erfc}\left(\lambda/\sqrt{\alpha_l}\right)} \left(\operatorname{erf}\left(\dfrac{x - s_0}{2\sqrt{\alpha_l t}}\right) - 1\right), & \text{if } x > s(t), \end{cases}$$

$$c(t,x) = \begin{cases} \underline{c}, & \text{if } x < s(t), \\ c_{liq} + \dfrac{c_{liq} - f_l^{-1} \circ f_s(\underline{c})}{\operatorname{erfc}\left(\lambda/\sqrt{D_l}\right)} \left(\operatorname{erf}\left(\dfrac{x - s_0}{2\sqrt{D_l t}}\right) - 1\right), & \text{if } x > s(t), \end{cases} \tag{39}$$

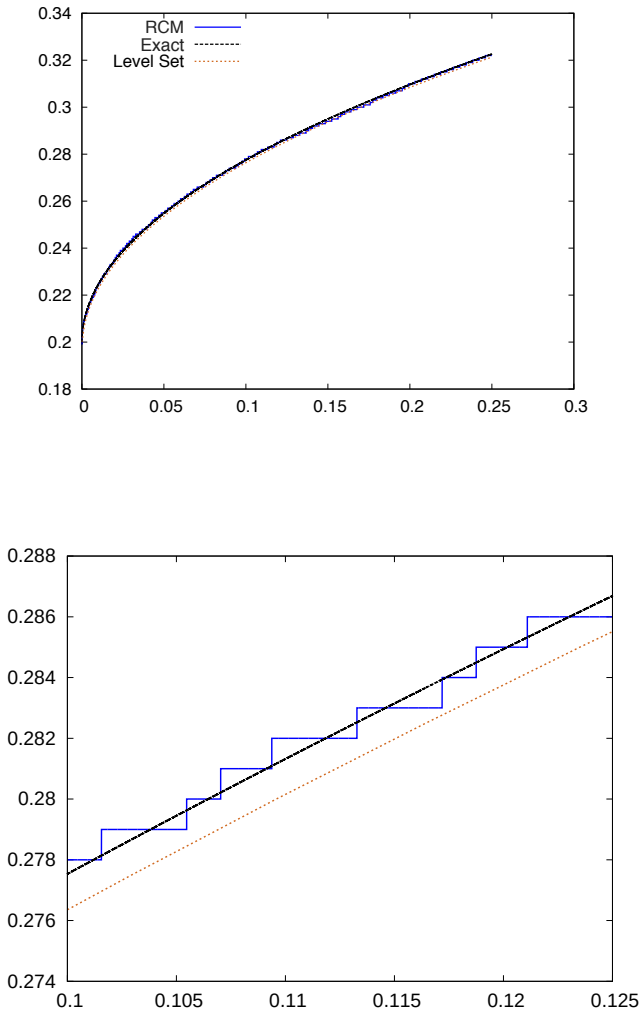

FIGURE 5. Comparison between level set and the random sampling method. Position of the interface in time and a zoom.

where $\alpha_k = K_k/(\rho c_{p,k})$, $k = l, s$ and the interface position reads $s(t) = s_0 + 2\lambda\sqrt{t}$. Considering a linear liquidus-solidus diagram, that is the liquidus and solidus functions are respectively given by $f_l(c) = T_A + \gamma_l c$ and $f_s(c) = T_A + \gamma_s c$ with $\gamma_l > \gamma_s$, one can determine the two constants $\lambda > 0$ and $\underline{c} \in [0, 1]$ by solving the

following nonlinear system

$$\begin{cases} \dfrac{c_{liq}-\overline{c}}{\underline{c}-\overline{c}} = \dfrac{\lambda \mathrm{erfc}\big(\lambda/\sqrt{D_l}\big)\sqrt{\pi D_l}}{\exp(\lambda^2/D_l)} =: H(\lambda), \\ T_{int} = \dfrac{L\lambda + T_{sol}A_1(\lambda) + T_{liq}A_2(\lambda)}{A_1(\lambda)+A_2(\lambda)} =: W(\lambda), \\ A_1(\lambda) := \dfrac{\sqrt{\alpha_s/\pi}\exp(-\lambda^2/\alpha_s)}{2-\mathrm{erfc}\big(\lambda/\sqrt{\alpha_s}\big)}, \\ A_2(\lambda) := \dfrac{\sqrt{\alpha_l/\pi}\exp(-\lambda^2/\alpha_l)}{\mathrm{erfc}\big(\lambda/\sqrt{\alpha_l}\big)}. \end{cases} \tag{40}$$

As it is proven in [26], the system (39)-(40) has a solution $(T_{int}, \underline{c}, \overline{c}, \lambda)$ with $T_A < T_{int} < T_{liq}$ and $0 < \overline{c} < \underline{c} < 1$ and $0 < \lambda$. The proof relies on the monotony of the continuous functions $W(\lambda)$ and $H(\lambda)$ (we refer to [26] for detailed arguments).

For the coefficients $\alpha_s = \alpha_l = D_s = D_l = \rho = L = 1$, $T_A = 2$, $\gamma_l = 2$, $\gamma_s = 1$, the temperatures $T_{liq} = 3$ and $T_{sol} = 0$ and the concentration $c_{liq} = 0.2$, the numerical resolution of (40) gives $\lambda = 0.1717126$, $\underline{c} = 0.3191531$, $\overline{c} = 0.1595766$ and $T_{int} = 2.3191531$.

To mimic the problem, we consider the initial temperature and concentration distribution

$$T(0,x) = \begin{cases} T_{sol}, & \text{if } 0 < x < s_0, \\ T_{int} = f_l(c_{liq}), & \text{if } x = s_0, \\ T_{liq}, & \text{if } s_0 < x < 5, \end{cases} \qquad c(0,x) = \begin{cases} \underline{c}, & \text{if } 0 < x < s_0, \\ c_{liq}, & \text{if } s_0 < x < 5, \end{cases}$$

where $s_0 = 1.665$ with homogeneous Neumann boundary conditions (for both the temperature and the concentration) on the finite domain $[0, 5]$. The computational domain contains 2000 cells and we fix $T_{final} = 0.1s$ and $CFL = 0.8$. The comparison between the Random Projection Method and the analytical solution are given in Figures 6. The computed concentration (Fig. 6-top) is in good agreement with the analytical solution, in particular the jump of concentration at the interface is sharp and well localized. Same observations can be done on the temperature field (Fig. 6-bottom): the computed temperature fits well the analytical temperature, the continuity of the temperature is properly preserved, the green mark indicates the interface. In Fig. 7-top, one observes the good agreement of position of the interface in time. Again the stepped profile of the curve is due to the Random Projection Method. The temperature of the interface in time is given in Fig. 7-middle. One observes that the algorithm requires few time iterations to capture the correct constant interface temperature T_{int}. The red dots correspond to the interface temperature recorded every 4000 time iterations. In Fig. 7-bottom, the corresponding solid concentrations $\underline{c}$ (red stars) and liquid concentrations $\overline{c}$ (red crosses) are plotted on the liquidus-solidus diagram. Except for the first time iterations, the computed concentrations are in good agreement with the liquidus-solidus diagram.

4.3. **A two interfaces test case.** We propose an academic test case where two interfaces evolve in the domain according to different liquidus-solidus diagrams plotted in Figure 10. The aim of the test case is to validate the ability of the Random Choice Method to handle two interfaces. The initial configuration consists in a liquid zone between two solid regions. The first interface obeys the liquidus-solidus diagram $f_{s,1}(c) = T_{A,1} + c$, $f_{l,1}(c) = T_{A,1} + 2c$ with $T_{A,1} = 2$ and the second interface follows $f_{s,2}(c) = T_{A,2} + 2c$, $f_{l,2}(c) = T_{A,2} + c$ with $T_{A,2} = 3.5$. We consider constant in space coefficients $\alpha_s = \alpha_l = D_s = D_l = \rho = L = 1$. We consider the

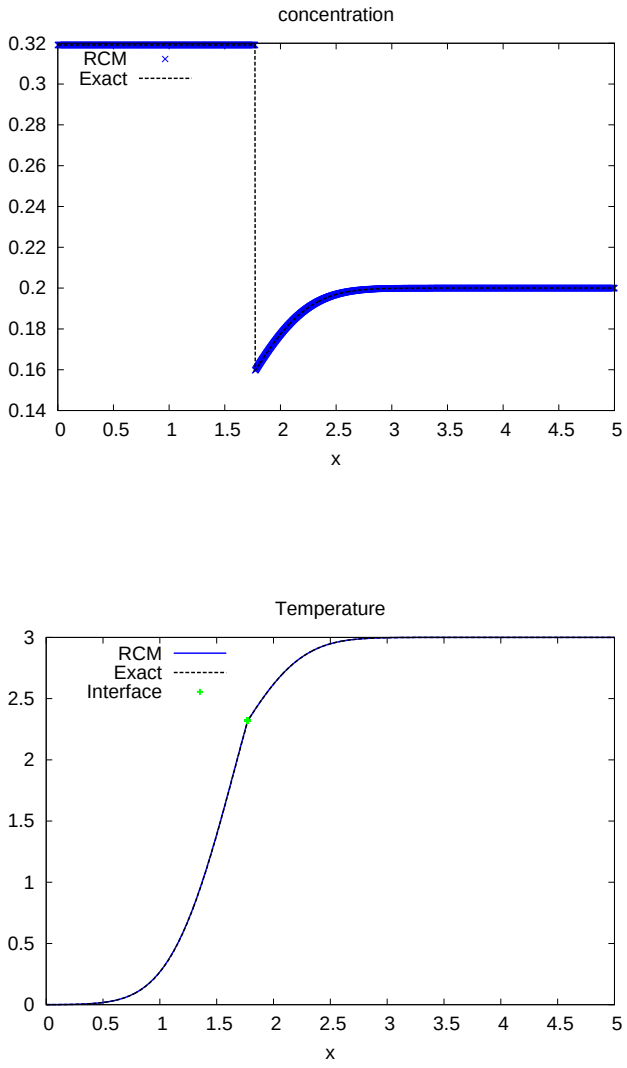

FIGURE 6. Comparison between the Random Projection Method and an analytical solution of the Rubinstein problem. From top to bottom: concentration profile in space, temperature profile in space.

initial profiles

$$T(0,x) = \begin{cases} 0, & \text{if } 0 < x < s_1, \\ 3, & \text{if } s_1 < x < s_2, \\ 4, & \text{if } s_2 < x < 5, \end{cases} \qquad c(0,x) = \begin{cases} 3.25 & \text{if } 0 < x < s_1, \\ 0.2, & \text{if } s_1 < x < s_2, \\ 0.1, & \text{if } s_2 < x < 5, \end{cases}$$

where $s_1 = 0.1$ and $s_2 = 1$ with homogeneous Neumann boundary conditions (for both the temperature and the concentration). Thus the first solid phase is increasing whereas the second decreases in time. The domain $[0, 5]$ is composed of 2000 cells, the computation time is $T_{final} = 0.1s$ and the CFL is 0.8. Note

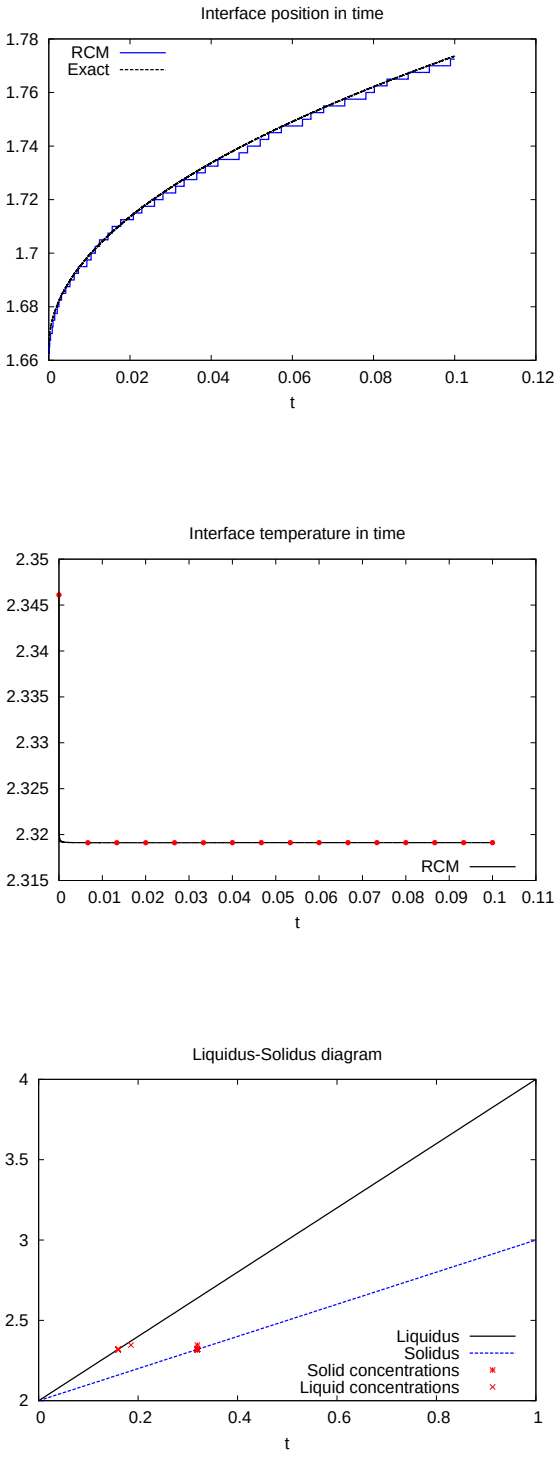

FIGURE 7. Comparison between the Random Projection Method and an analytical solution of the Rubinstein problem. From top to bottom: position of the interface in time, temperature of the interface in time, computed concentrations $\underline{c}$ and $\overline{c}$ and correspondance with the liquidus-solidus diagram.

that the time step is submitted to the stability conditions (23)-(33)-(34) of both interfaces. The concentration and the temperature profiles are given in Figure 8. Once again one observes that the jump of concentrations are accurately located and the continuity of the temperature is preserved. The evolutions of the interfaces in time are given in Figure 9-top. The first solid phase increasing slowly whereas the decrease of the second solid phase is much faster. The temperatures of both interfaces achieve a constant value rapidly ($T_{int,1} = 3.65$ and $T_{int,2} = 2.28$). Each dot on the temperature curves in time correspond to liquid and solid concentrations plotted on the liquidus-solidus diagrams in Figure 10.

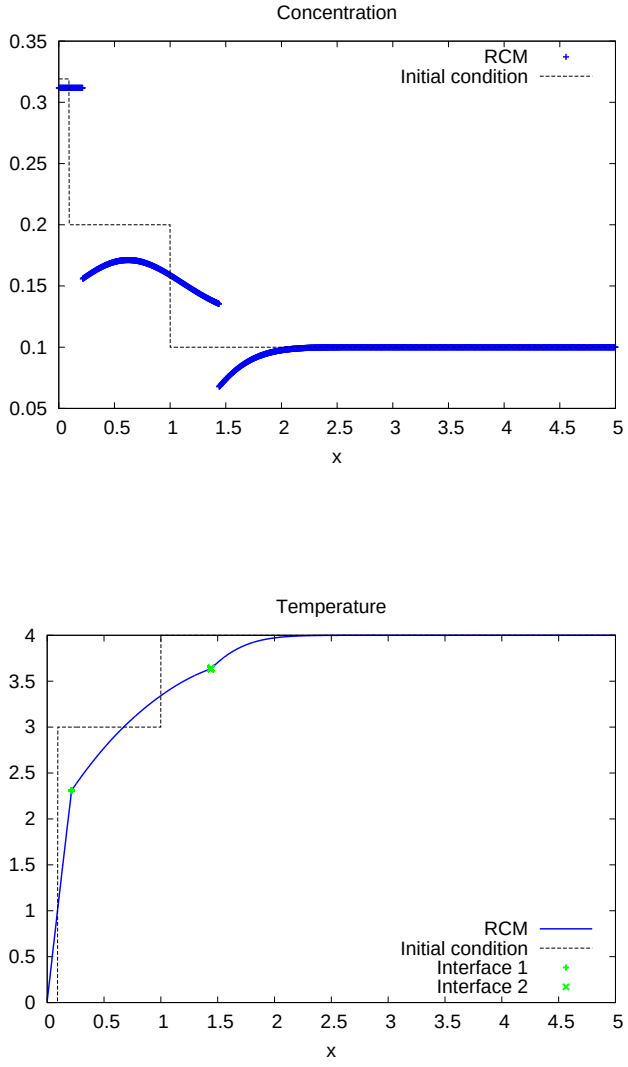

FIGURE 8. Two interfaces test case. From top to bottom: concentration profile in space, temperature profile in space.

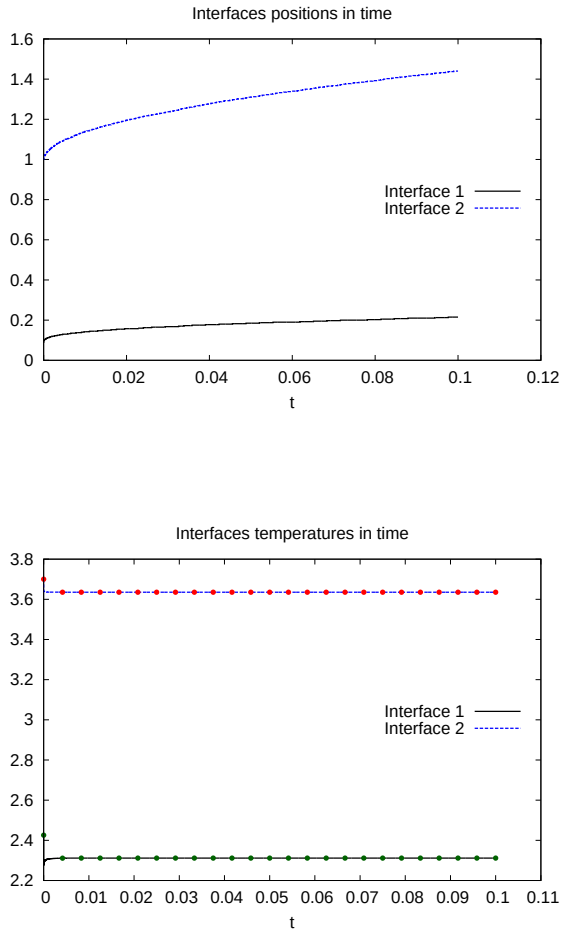

FIGURE 9. Two interfaces test case. From top to bottom: position of the interfaces in time, temperatures of the interfaces in time and computed concentrations $\underline{c}$ and $\overline{c}$.

5. Conclusion

In this paper we proposed a Lagrange projection scheme for the Rubinstein and Stefan-like problems. The Lagrangian step relies on the definition of proper numerical fluxes which guarantee by construction the continuity of the temperature and the jump of the concentration according to an noneutectic liquidus-solidus diagram. The projection step is performed at the interface only by a random sampling technique. The numerical scheme exhibits good properties (stability, maximum principle) and provides good numerical results compared to the level set method and analytical solutions. Our perspectives are in several directions:

- get rid of the explicit time integration and CFL constraints to adopt an implicit time integration;
- extend the random choice method to higher dimension by a simple directional splitting algorithm. This could be performed on cartesian grids as soon as the interface does not present a dendritic profile;

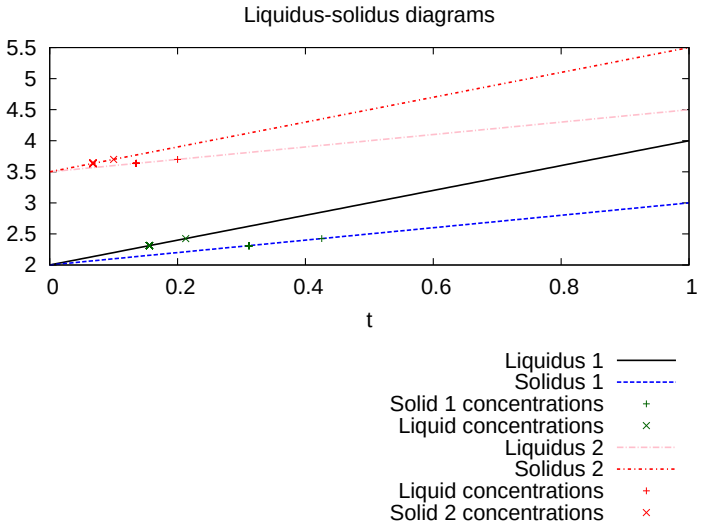

FIGURE 10. Two interfaces test case. Computed concentrations $\underline{c}$ and $\overline{c}$ for both interfaces and correspondance with the liquidus-solidus diagrams.

- enrich the model to take into account convection in the domain. This will modify the definition of the numerical fluxes for the temperature field but won't modify the random projection step.

Acknowledgments. This work has been supported by the TELLUS INSMI-INSU CNRS program.

REFERENCES

[1] V. Alexiades, D. G. Wilson, and A. D. Solomon. Macroscopic global modeling of binary alloy solidification processes. *Quart. Appl. Math.*, 43(2):143–158, 1985.

[2] B. Andreianov, F. Lagoutière, T. Takahashi, and S. Seguin. Small solids in an inviscid fluid. *INetw. Heterog. Media*, 5:385–404, 2010.

[3] M. Bachmann, P. Helluy, J. Jung, H. Mathis, and S. Müller. Random sampling remap for compressible two-phase flows. *Comput. & Fluids*, 86:275–283, 2013.

[4] C. Bui, Ch. Dapogny, and P. Frey. An accurate anisotropic adaptation method for solving the level set advection equation. *Int. J. Numer. Meth. Fluids*, 2012.

[5] G. Caginalp and W. Xie. Phase-field and sharp-interface alloy models. *Phys. Rev. E (3)*, 48(3):1897–1909, 1993.

[6] C. Chalons. Transport-equilibrium schemes for computing nonclassical shocks. *C. R. Math. Acad. Sci. Paris*, 342(8):623–626, 2006.

[7] C. Chalons and F. Coquel. Numerical capture of shock solutions of nonconservative hyperbolic systems via kinetic functions. In *Analysis and simulation of fluid dynamics*, Adv. Math. Fluid Mech., pages 45–68. Birkhäuser, Basel, 2007.

[8] C. Chalons and P. Goatin. Godunov scheme and sampling technique for computing phase transitions in traffic flow modeling. *Interfaces Free Bound.*, 10(2):197–221, 2008.

[9] S. Chen, B. Merriman, S. Osher, and P. Smereka. A simple level set method for solving stefan problems. *J. Comp. Phys.*, 1997.

[10] Ch. Dapogny and P. Frey. Computation of the signed distance function to a discrete contour on adapted triangulation. *Calcolo*, 2012.

[11] W. Dreyer and B. Wagner. Sharp-interface model for eutectic alloys. I. Concentration dependent surface tension. *Interfaces Free Bound.*, 7(2):199–227, 2005.

[12] J. Glimm. Solutions in the large for nonlinear hyperbolic systems of equations. *Comm. Pure Appl. Math.*, 18:697–715, 1965.
[13] O. Grasset and E.M. Parmentier. Thermal convection in a infinite prandtl number, strongly temperature dependent, volumetrically heated fluid: implications for planetary thermal evolution. *J. Geophys. Res.*, 1998.
[14] P. Helluy and J. Jung. Two-fluid compressible simulations on GPU cluster. In *Congrès SMAI 2013*, volume 45 of *ESAIM Proc. Surveys*, pages 349–358. EDP Sci., Les Ulis, 2014.
[15] E. Javierre, C. Vuik, F.J. Vermolen, and S. van der Zwaag. A comparison of numerical models for one-dimensional stefan problems. *J. Comput. Appl. Math.*, 2006.
[16] L. I. Rubinstein. *The Stefan problem*. American Mathematical Society, Providence, R.I., 1971. Translated from the Russian by A. D. Solomon, Translations of Mathematical Monographs, Vol. 27.
[17] A. Showman, D.J. Stevenson, and R. Mahlotra. Coupled orbital and thermal evolution of ganymede. *Icarus*, 1997.
[18] D. A. Tarzia. Neumann-like solution for the two-phase stefan problem with a simple mushy zone model. *Computational and Applied Mathematics*, 1990.
[19] D. A. Tarzia. *A bibliography on moving-free boundary problems for the heat-diffusion equation. The Stefan and related problems*, volume 2 of *MAT. Serie A: Conferencias, Seminarios y Trabajos de Matemática [MAT. Series A: Mathematical Conferences, Seminars and Papers]*. Universidad Austral, Facultad de Ciencias Empresariales (FCE-UA), Departamento de Matemática, Rosario, 2000.
[20] M. Theillard, F. Gibou, and T. Pollock. A sharp computational method for the simulation of the solidification of binary alloys. *J. Sci. Comput.*, 63(2):330–354, 2015.
[21] G. Tobie, A. Mocquet, and C. Sotin. Tidal dissipation within large icy satellites: Application to europa and titan. *Icarus*, 2005.
[22] A. Visintin. Phase transitions and glass formation in binary alloys. *SIAM J. Math. Anal.*, 41(5):1725–1756, 2009.
[23] V.R. Voller. An implicit enthalpy solution for phase change problems: with application to a binary alloy solidification. *Applied Mathematical Modelling*, 11(2):110 – 116, 1987.
[24] V.R. Voller. A numerical method for the rubinstein binary-alloy problem in the presence of an uncer-cooled liquid. *International Journal of Heat and Mass Transfer*, 51(2):696 – 706, 2008.
[25] V.R. Voller, A. Mouchmov, and M. Cross. An explicit scheme for coupling temperature and concentration fields in solidification models. *Applied Mathematical Modelling*, 28(1):79 – 94, 2004. Mathematical Modelling in Metals Processing.
[26] D. G. Wilson, A. D. Solomon, and V. Alexiades. A model of binary alloy solidification. *Internat. J. Numer. Methods Engrg.*, 20(6):1067–1084, 1984.

(Sabrina Carpy) Laboratoire de Planétologie et Géodynamique de Nantes, Université de Nantes & CNRS UMR 6112, BP 92208, F-44322 Nantes Cedex 3, France
E-mail address: sabrina.carpy@univ-nantes.fr

(Hélène Mathis) Laboratoire Jean Leray, Université de Nantes & CNRS UMR 6629, BP 92208, F-44322 Nantes Cedex 3, France
E-mail address, Corresponding author: helene.mathis@univ-nantes.fr